Available online at www.sciencedirect.com
ScienceDirect
Journal of Sound and Vibration 300 (2007) 176–196
JOURNAL OF SOUND AND VIBRATION
www.elsevier.com/locate/jsvi

Vibration control of pre-twisted rotating composite thin-walled beams with piezoelectric fiber composites

Seung-Chan Choi[1], Jae-Sang Park, Ji-Hwan Kim*

School of Mechanical and Aerospace Engineering, Seoul National University, Institute of Advanced Aerospace Technology, San 56-1, Sillim-Dong, Gwanak-Gu, Seoul 151-742, Republic of Korea

Received 17 January 2005; received in revised form 7 July 2006; accepted 24 July 2006
Available online 21 November 2006

Abstract

Rotating composite beam structures like blades are applied in many fields of aerospace and mechanical engineering. In this research, bending vibration control of the pre-twisted rotating composite thin-walled beam is studied. The formulation is based on single cell composite beam including a warping function, centrifugal force, Coriolis acceleration, pre-twist angle and piezoelectric effect. A negative velocity feedback control algorithm is applied to realize the adaptive capability of the beam. Using a finite-element method, numerical simulations show that macro-fiber composite (MFC) actuators which are piezoelectric fiber composites and PVDF sensors can generate active vibration control effect. Relations between active vibration control effect and design parameters of beams such as rotating speeds, pre-twist angles and fiber orientations in a host structure are investigated in detail. Besides, a case study conformed that the effective damping performance can be obtained by suitable arrangement and distribution of the sensor and actuator pairs.

1. Introduction

Thin-walled beams are applied in many fields of aerospace and mechanical industry. Helicopter blades, tilt-rotor aircraft blades, flexible robot arms and wind turbines are representative examples of structures that have the shape of a thin-walled beam. Recently, composite materials have been widely used in these structures, obtaining an increased specific stiffness and specific strength. Because composite structures possess flexible characteristics, vibration suppression has emerged as an important problem in determining the operating quality of the system. Vibration suppression methods are classified into passive method and active method. Recently, the later has been focus of research, because it can be allowed the adaptability according to circumstances.

Numerous researches have been conducted on composite thin-walled beams. Rehfield [1] studied the design analysis methodology of a thin-walled beam for composite rotor blades. Rehfield et al. [2] discussed the

*Corresponding author. Tel.: +82 2 880 7383; fax: +82 2 887 2662.
E-mail address: jwhkim@snu.ac.kr (J.-H. Kim).
[1]Current address: Corporate Research & Development Division, Advanced Technology Center, Hyundai-Kia Motors 772-1, Jangduk-dong, Hwaseong-Si, Gyeonggi-Do 445-706, Republic of Korea.

0022-460X/$ - see front matter © 2006 Elsevier Ltd. All rights reserved.
doi:10.1016/j.jsv.2006.07.051

non-classical behavior of thin-walled composite beams with closed cross sections. Chandra and Chopra [3] investigated the vibration characteristics of rotating composite box beams by experiment and theoretical methods. Smith and Chopra [4] researched the aeroelastic response, loads and stability of a composite thin-walled beam whereas Song and Librescu [5] studied the free vibration of anisotropic composite thin-walled beams with a closed cross-section contour using an extended Galerkin method. In addition, Stemple and Lee [6] investigated composite beams undergoing a large deflection with arbitrary cross-section warping using a finite element method. Also, Oh et al. [7] discussed the effects of pretwisted and presetting angle of rotating thin-walled composite beam.

Research has been intensifying over the past two decades regarding active vibration control methods for structures by use of smart materials. The potential and suitability of using smart composite structures for active suppression of vibration in aerospace industry is a widely investigated topic of research. The most widely used smart materials for vibration control in structures are piezoelectric materials since it has desirable characteristics; fast response and covering a broad range of frequency. They generate an electric charge when subject to a mechanical deformation, which is called the direct piezoelectric effect. Conversely, mechanical stress or strain is produced by applied electric field, which is called the converse piezoelectric effect. These properties allow piezoelectric materials to act as distributed sensors and actuators in the active control of dynamic systems. Reddy [8] proposed theoretical formulations and finite element models for laminated composite plates with integrated piezoelectric sensors and actuators based on the classical and shear deformation plate theories. Lam et al. [9] studied a finite-element model of a composite laminated plate with distributed piezoelectric sensors and actuators for active vibration control using a negative velocity feedback control algorithm. In his study, the static analysis of a piezoelectric actuation and active vibration suppression of a cantilevered composite plate are performed as a numerical simulation. Further, Mukherjee et al. [10] presented a general formulation for active vibration control for a stiffened plate with piezoelectric actuators through a negative velocity feedback control and investigated the influence of the position of stiffener.

Also, a rotating active beam using piezoelectric materials has been studied. Song et al. [11] researched the vibration of rotating blades modeled as anisotropic thin-walled beams containing piezoelectric materials through the proportional control law and velocity control law. Chandiramani et al. [12] discussed optimal vibration control of a rotating composite beam with distributed piezoelectric sensing and actuation. They presented the numerical simulation for a time varying load that is often applied to structures such as rotor blades. Also, Koldoff et al. [13] studied the active control of a composite box beam using surface bonded piezoelectric materials actuation for individual blade control (IBC). Further, Choi and Han [14] gave a concrete expression for the vibration control of the rotating cantilevered beam using piezo-actuator in an experimental method.

The most widely used piezoceramics (such as lead zirconate titanate: PZT) for vibration control are in the form of thin sheet that can be readily embedded or attached to composite structures. However, the typical piezoceramic actuator has some disadvantages. They have the brittleness of piezoceramics which makes them vulnerable to damage. In addition, they can hardly conform to the curved surface. To overcome these drawbacks of a typical piezoceramic actuator, active fiber composite (AFC) actuator was introduced by Bent [15] and macro-fiber composite (MFC) actuator was developed by Wilkie et al. [16] recently. These piezo-composite materials consist of the piezoceramic fiber, epoxy matrix and interdigitated electrode. In addition, they have advantages as follows. Piezo-composite materials can utilize the d_{11} piezoelectric constant to the direction of piezoceramic fibers which is larger than the d_{31} piezoelectric constant of the typical piezoceramic actuator. Also, the polymer matrix can protect piezoceramic fibers against the impact and it makes piezo-composite materials flexible. Therefore, they can conform to the curved surface easily. These advantages of piezo-composite materials can be applied to more practical applications of smart structure technology. Further, piezo-composite materials can produce a twisting actuation due to the anisotropic characteristics; difficult to achieve using the typical piezoceramic actuator. Plessis and Hagood [17] studied the modeling and experimental testing of twist actuated single cell composite beam using AFC for blade control. Cesnik and Shin [18] studied the vibration problem in a helicopter rotor blade using AFC for active individual blade control. Also, Sheta et al. [19] researched active control of F/A-18 vertical tail buffeting using MFC actuators.

Till now, general piezoceramic actuators have been widely adopted in the reduction and control of the bending vibration for rotating beam structures. In the present study, piezoelectric fiber composite actuators are

selected and, main aim is to improve the damping performance for bending vibration control of the rotating composite thin-walled beam using MFC actuators and PVDF sensors. The formulation for vibration control of the beams is based on the single cell composite beam, including a warping function, centrifugal force, Coriolis acceleration, pretwist angle and piezoelectric effect. A negative velocity feedback control algorithm coupling the direct and converse piezoelectric effects is used to actively control the dynamic response of the structure through a closed control loop. Numerical studies based on a finite element method are performed, and dynamic responses of the beam are analyzed. The effects of feedback control gain on damping performance are examined in detail. Furthermore, influences of parameters, such as rotating speeds, pre-twist angles of the beam, and fiber orientations in host structure are investigated. Also, a case study confirmed effective damping performance by the suitable arrangement and distribution of sensor and actuator pairs.

2. Formulation

2.1. Basic assumptions

In this study, we will use the following assumptions for modeling of the thin-walled, single cell, composite beam [1,17]:

(1) Cross-sectional shape is maintained during deformation but out-of-plane displacement is allowed.
(2) Wall thickness is small compared to other dimensions so that the problem can treated as a thin-walled, plane stress problem.
(3) The transverse in-plane normal stresses are negligible (no internal pressure).
(4) Rate of twist can vary along the length of beam and it acts as a measure of the torsional warping of the cross section.

2.2. Kinematics

Fig. 1 describes the rotating flexible beam model. The origin of the rotating axis system (X, Y, Z) is located at the root of the beam, and R_0 is the radius of the rigid hub. Also, the beam rotates about its polar axis through the origin O. The length of the beam is l with the constant rotating speed Ω, and the local coordinate system (X_p, Y_p, Z_p) is defined as the principal axes of an arbitrary beam cross section as shown in the figure. The transformation formulas between two coordinate systems (X, Y, Z) and (X_p, Y_p, Z_p) are as follows:

$$\begin{Bmatrix} X \\ Y \\ Z \end{Bmatrix} = \begin{bmatrix} 1 & 0 & 0 \\ 0 & \cos\beta(x) & -\sin\beta(x) \\ 0 & \sin\beta(x) & \cos\beta(x) \end{bmatrix} \begin{Bmatrix} X^p \\ Y^p \\ Z^p \end{Bmatrix}, \tag{1}$$

where $\beta(x) = \gamma + \beta_0(x/l)$.

In Eq. (1), γ is the setting angle, β_0 is the pre-twist angle per unit blade length, and $\beta(x)$ is the pre-twist angle in the arbitrary section.

The fixed coordinate system ($\underline{X}$, $\underline{Y}$, $\underline{Z}$) is attached to the center of the hub that is to say at O. In addition, the local Cartesian coordinate system (x, t, n) is located at the mid-plane of the cross-section of the laminate beam wall and moves around the contour with circumferential coordinate s. In the local coordinate system, t is the tangential coordinate and n is the outward normal coordinate.

Also, the position, velocity and acceleration vectors for the deformed structure are described as [22]

$$\begin{aligned} \bar{\mathbf{R}} &= (x+u+R_0)\mathbf{i} + (y+v)\mathbf{j} + (z+w)\mathbf{k}, \\ \bar{\mathbf{v}} &= (\dot{u} - \Omega(y+v))\mathbf{i} + \Omega(\dot{v} + (x+u+R_0))\mathbf{j} + \dot{w}\mathbf{k}, \\ \bar{\mathbf{a}} &= \left(\ddot{u} - 2\Omega\dot{v} - \Omega^2(x+u+R_0)\right)\mathbf{i} \\ &\quad + \left((\ddot{v} + 2\Omega\dot{u} - \Omega^2(y+v)\right)\mathbf{j} + \ddot{w}\mathbf{k}. \end{aligned} \tag{2}$$

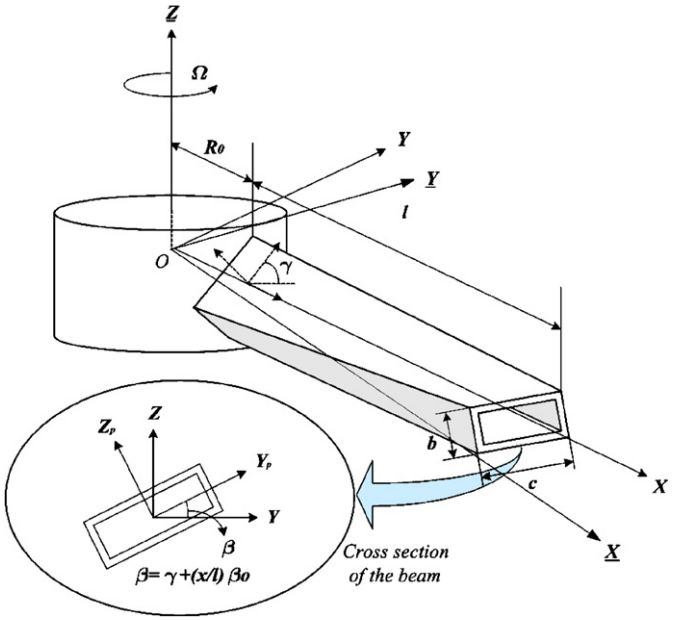

Fig. 1. Rotating composite thin-walled beam.

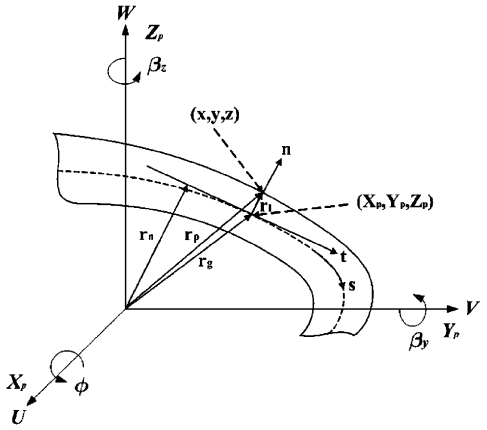

Fig. 2. Position vector of a point in the beam wall.

2.2.1. Displacement fields

To reduce the three-dimensional (3D) elastic problem to an equivalent 1D one, the components of displacement are considered according to basic assumptions [17,22]:

$$\begin{aligned} u(x) &= U(x) - (Y - nZ_{,s})\beta_z(x) + (Z + nY_{,s})\beta_y(x) + \psi(s)\phi_{,x}(x), \\ v(x) &= V(x) - (Z + nY_{,s})\phi(x), \\ w(x) &= W(x) + (Y - nZ_{,s})\phi(x). \end{aligned} \tag{3}$$

In these equations, global displacements u, v and w of any point in the beam wall can be given in terms of the cross-sectional displacement values as shown in Fig. 2, $U(x)$, $V(x)$, $W(x)$, the cross-sectional rotation $\phi(x)$, $\beta_y(x)$, $\beta_z(x)$, the beam twist rate $\phi_{,x}$, respectively. Also, the torsional warping function, $\psi(x)$ is considered as

$$\psi(s) = \frac{-2A}{\Gamma}\int_0^s \alpha\,\mathrm{d}s + \int_0^s r_n\,\mathrm{d}s, \tag{4}$$

where A is the cross-sectional area, α the warping parameter, and r_n the normal projection of the mid-plane position vector on the unit normal vector as shown in Fig. 3. Further, Γ represents both the contour and the actual mid-plane contour length.

2.2.2. Strain-displacement relations

The axial normal strain is decomposed into the mid-plane strain and the local bending curvature strain as [22]

$$\varepsilon_{xx} = U_{,x} - Y\beta_{z,x} + Z\beta_{y,x} + \psi\phi_{,xx} + n(Y_{,s}\beta_{y,x} + Z_{,s}\beta_{z,x}) = \varepsilon^o_{xx} + n\kappa_{xx}. \tag{5}$$

The shear strain in the wall of the beam is constant and is not a function of the thickness coordinate n. Thus

$$\gamma_{xs} = (V_{,x} - \beta_z)Y_{,s} + (W_{,x} + \beta_y)Z_{,s} - \frac{2A\alpha\phi_{,x}}{\Gamma} = \gamma_{xy}Y_{,s} + \gamma_{xz}Z_{,s} - \frac{2A}{\Gamma}\alpha\phi_{,x} = \gamma^o_{xs} \tag{6}$$

Therefore, the strain vector can be represented as

$$\begin{Bmatrix} \varepsilon_{xx} \\ \varepsilon_{ss} \\ \gamma_{xs} \end{Bmatrix} = \begin{Bmatrix} \varepsilon^o_{xx} \\ \varepsilon^o_{ss} \\ \gamma^o_{xs} \end{Bmatrix} + n\begin{Bmatrix} \kappa_{xx} \\ \kappa_{ss} \\ \kappa_{xs} \end{Bmatrix} = \varepsilon^o + n\boldsymbol{\kappa}. \tag{7}$$

2.3. Constitutive relations

The beam is composed of composite materials. They consist of the passive material which is host structures and the active material which is sensors and actuators. It is considered that both passive and active materials used for beam construction can be modeled with the linear piezoelectric constitutive relationships as

$$\mathbf{D} = \mathbf{e}\,\boldsymbol{\varepsilon} + \in \mathbf{E}, \tag{8a}$$

$$\boldsymbol{\sigma} = \mathbf{C}\,\boldsymbol{\varepsilon} - \mathbf{e}^{\mathrm{T}}\,\mathbf{E}, \tag{8b}$$

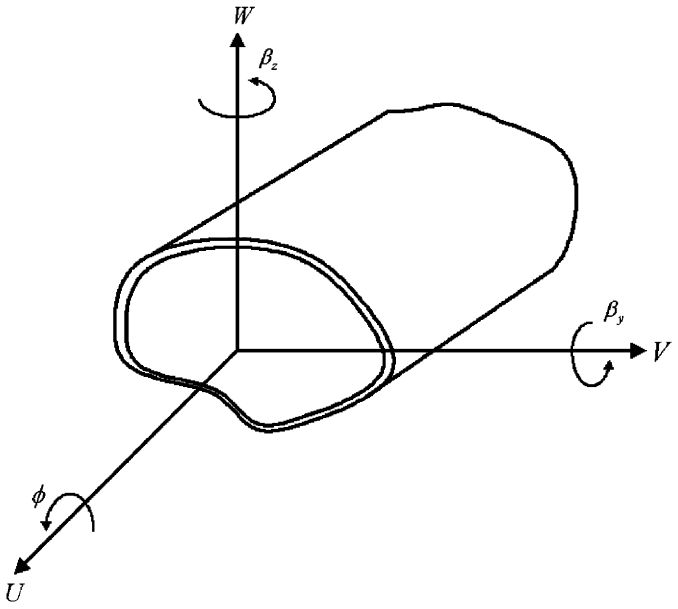

Fig. 3. Displacement variables of thin-walled beam.

where $\boldsymbol{\varepsilon}$, $\boldsymbol{\sigma}$, $\mathbf{D}$ and $\mathbf{E}$ are strain, stress, electric displacement and electric field vectors, respectively. While $\mathbf{e}$, $\in$ and $\mathbf{C}$ are piezoelectric constants, permittivity coefficients and material elastic coefficient, respectively. Eq. (8a) describes the 'direct piezoelectric effect' and Eq. (8b) describes the 'converse piezoelectric effect'.

The standard notation for composite materials is used instead of the standard piezoelectric notation in this study. Fiber-reinforced composite materials and piezo-composite materials have transversely isotropic characteristics. For transversely isotropic materials, there are only five independent stiffness coefficients as follows:

$$\begin{Bmatrix} \sigma_{11} \\ \sigma_{22} \\ \sigma_{33} \\ \tau_{23} \\ \tau_{31} \\ \tau_{12} \end{Bmatrix} = \begin{bmatrix} C_{11} & C_{12} & C_{12} & 0 & 0 & 0 \\ C_{12} & C_{22} & C_{23} & 0 & 0 & 0 \\ C_{12} & C_{23} & C_{22} & 0 & 0 & 0 \\ 0 & 0 & 0 & \frac{C_{22}-C_{23}}{2} & 0 & 0 \\ 0 & 0 & 0 & 0 & C_{66} & 0 \\ 0 & 0 & 0 & 0 & 0 & C_{66} \end{bmatrix} \begin{Bmatrix} \varepsilon_{11} \\ \varepsilon_{22} \\ \varepsilon_{33} \\ \gamma_{23} \\ \gamma_{31} \\ \gamma_{12} \end{Bmatrix} - \begin{bmatrix} e_{11} \\ e_{12} \\ e_{13} \\ 0 \\ 0 \\ 0 \end{bmatrix} E_1. \tag{9}$$

Further, the important stresses for thin-walled composite beams are the normal stresses and the in-plane shear stress in the laminate walls. Though the stress in the through-thickness direction exist, they are small. Therefore the problem can treated as a plane stress problem with [20],

$$\sigma_{33} = 0, \tau_{23} = 0, \text{ and } \tau_{31} = 0.$$

The reduced constitutive relation is

$$\begin{Bmatrix} \sigma_{11} \\ \sigma_{22} \\ \tau_{12} \end{Bmatrix} = \begin{bmatrix} Q_{11} & Q_{12} & 0 \\ Q_{12} & Q_{22} & 0 \\ 0 & 0 & Q_{66} \end{bmatrix} \begin{Bmatrix} \varepsilon_{11} \\ \varepsilon_{22} \\ \gamma_{12} \end{Bmatrix} - \begin{bmatrix} e_{11}^* \\ e_{12}^* \\ 0 \end{bmatrix} E_1. \tag{10}$$

Also, transformed reduced constitutive relation for the fiber orientation is obtained as follows:

$$\boldsymbol{\sigma}_k = \begin{Bmatrix} \sigma_{xx} \\ \sigma_{ss} \\ \tau_{xs} \end{Bmatrix}_k = \begin{bmatrix} \bar{Q}_{11} & \bar{Q}_{12} & \bar{Q}_{16} \\ \bar{Q}_{12} & \bar{Q}_{22} & \bar{Q}_{26} \\ \bar{Q}_{16} & \bar{Q}_{26} & \bar{Q}_{66} \end{bmatrix}_k \begin{Bmatrix} \varepsilon_{xx} \\ \varepsilon_{ss} \\ \gamma_{xs} \end{Bmatrix} - \begin{bmatrix} \bar{e}_{xx} \\ \bar{e}_{ss} \\ \bar{e}_{xs} \end{bmatrix}_k E_{1k}. \tag{11}$$

The electric field is defined as $E_{1_k} = -(V_k/p_k)$, where V_k and p_k are the applied voltage and electrode spacing of the interdigitated electrode for the kth layer, respectively.

The force and moment resultant vectors are defined as

$$(\mathbf{N}, \quad \mathbf{M}) = \int_{-h/2}^{h/2} \boldsymbol{\sigma}(1, \quad n)\, \mathrm{d}n. \tag{12}$$

Therefore, the constitutive equation can be represented as

$$\begin{Bmatrix} \mathbf{N} \\ \mathbf{M} \end{Bmatrix} = \begin{bmatrix} \mathbf{A} & \mathbf{B} \\ \mathbf{B} & \mathbf{D} \end{bmatrix} \begin{Bmatrix} \boldsymbol{\varepsilon}^o \\ \boldsymbol{\kappa} \end{Bmatrix} - \begin{Bmatrix} \mathbf{N}^a \\ \mathbf{M}^a \end{Bmatrix}. \tag{13}$$

Since the hoop stress σ_s is zero, N_s is zero. In addition, the cross-section is infinitely rigid in its own plane which results in zero transverse and twisting curvatures (κ_s, $\kappa_{xs} = 0$). Therefore, Eq. (13) can be reduced as

$$\begin{Bmatrix} N_{xx} \\ N_{xs} \\ M_{xx} \end{Bmatrix} = \begin{bmatrix} L_{11} & L_{12} & L_{13} \\ L_{12} & L_{22} & L_{23} \\ L_{13} & L_{23} & L_{33} \end{bmatrix} \begin{Bmatrix} \varepsilon_{xx}^0 \\ \gamma_{xs}^0 \\ \kappa_{xx} \end{Bmatrix} - \begin{Bmatrix} \bar{N}_{xx}^a \\ \bar{N}_{xs}^a \\ \bar{M}_{xx}^a \end{Bmatrix} = \mathbf{L}\,\boldsymbol{\varepsilon} - \mathbf{P}\,\mathbf{E}_1, \tag{14}$$

where the reduced laminate stiffness and piezoelectric stress resultant are defined as

$$L_{11} = A_{11} - \frac{A_{12}^2}{A_{22}},\ L_{12} = A_{16} - \frac{A_{12}A_{26}}{A_{22}},\ L_{13} = B_{11} - \frac{A_{12}B_{12}}{A_{22}},$$
$$L_{22} = A_{66} - \frac{A_{26}^2}{A_{22}},\ L_{23} = B_{16} - \frac{A_{26}B_{12}}{A_{22}},\ L_{33} = D_{11} - \frac{B_{12}^2}{A_{22}},$$
$$\bar{N}_{xx}^a = N_{xx}^a - \frac{A_{12}}{A_{22}}N_{ss}^a,\ \bar{N}_{xs}^a = N_{xs}^a - \frac{A_{26}}{A_{22}}N_{ss}^a,$$
$$\bar{M}_{xx}^a = M_{xx}^a - \frac{B_{12}}{A_{22}}N_{ss}^a. \tag{15}$$

2.4. Governing equation including negative velocity feedback control

The strain energy due to deformation of composite beam can be written as

$$U_1 = \frac{1}{2}\int_0^l \oint_\Gamma \left(N_{xx}\varepsilon_{xx}^0 + N_{xs}\gamma_{xs} + M_{xx}\kappa_{xx}\right) \mathrm{d}s\,\mathrm{d}x. \tag{16}$$

When the beam rotates, a centrifugal force exists as [22]

$$F_{\mathrm{CF}}(x) = \int_x^l \rho\bar{A}\Omega^2(R_0 + x)\,\mathrm{d}x = \rho\bar{A}\Omega^2\left[R_0(L-x) + \frac{1}{2}\left(L^2 - x^2\right)\right], \tag{17}$$

where $\bar{A}$ is the real area of the cross-section, and ρ is the density of beams.

The strain energy due to the rotating motion of the beam can be written as

$$U_2 = \frac{1}{2}\int_0^l F_{\mathrm{CF}}(x)\left(\frac{\partial V}{\partial x}\right)^2 \mathrm{d}x + \frac{1}{2}\int_0^l F_{\mathrm{CF}}(x)\left(\frac{\partial W}{\partial x}\right)^2 \mathrm{d}x. \tag{18}$$

Then, the total strain energy is expressed as follows [15,16]:

$$U = U_1 + U_2. \tag{19}$$

Further, the kinetic energy with the rotating motion is

$$T = \frac{1}{2}\int_0^l \oint_\Gamma \int_h \rho\bar{\mathbf{v}}\cdot\bar{\mathbf{v}}\,\mathrm{d}n\,\mathrm{d}s\,\mathrm{d}x. \tag{20}$$

To derive the governing equation, the Hamilton's principle is adopted as

$$\int_{t_1}^{t_2} (\delta T - \delta U + \delta W)\,\mathrm{d}t = 0. \tag{21}$$

The variation of the strain energy U, kinetic energy T and external work W can be written as

$$\delta U = \int_0^l \oint_\Gamma \delta\boldsymbol{\varepsilon}^{\mathrm{T}}\{\mathbf{L}\,\boldsymbol{\varepsilon} - \mathbf{P}\mathbf{E}_1\}\,\mathrm{d}s\,\mathrm{d}x + \delta U_2 = \int_0^l \oint_\Gamma \delta\mathbf{q}^{\mathrm{T}}\left\{\mathbf{B}_u^{\mathrm{T}}\mathbf{L}\mathbf{B}_u\mathbf{q} - \mathbf{B}_u^{\mathrm{T}}\mathbf{P}\mathbf{E}_1\right\}\mathrm{d}s\,\mathrm{d}x + \delta U_2, \tag{22}$$

$$\delta T = -\int_0^l \oint_\Gamma \delta\mathbf{q}^{\mathrm{T}}\left\{\bar{P}_m + \bar{P}_c + \bar{P}_{cf} + \bar{F}_{cf}\right\}\mathrm{d}s\,\mathrm{d}x, \tag{23}$$

$$\delta W = \int_0^l \delta\mathbf{q}^{\mathrm{T}}\mathbf{N}_u\mathbf{f}\,\mathrm{d}x, \tag{24}$$

where $\mathbf{B}_u$, $\mathbf{N}_u$, $\mathbf{q}$, and $\mathbf{f}$ are the strain interpolation matrix, the displacement interpolation matrix, the nodal displacement vector and external force vector, respectively.

Finally, the equation of motion can be derived as

$$\mathbf{M}\ddot{\mathbf{q}}(t) + \mathbf{C}_C\dot{\mathbf{q}}(t) + (\mathbf{K}_L + \mathbf{K}_{\mathrm{CF}} + \mathbf{K}_G)\mathbf{q}(t) = \mathbf{F}_v + \mathbf{F}_{\mathrm{CF}} + \mathbf{R}(t), \tag{25}$$

where, $\mathbf{M}$, $\mathbf{C}_C$, $\mathbf{K}_L$, $\mathbf{K}_{\mathrm{CF}}$, $\mathbf{K}_G$, $\mathbf{F}_{\mathrm{CF}}$ and $\mathbf{R}(t)$ are the mass matrix, the Coriolis matrix, the linear stiffness matrix, the stiffness matrix due to centrifugal force, the geometric stiffness matrix, centrifugal force vector and arbitrary load, respectively. Also, dimensions of $\mathbf{M}$, $\mathbf{C}_C$, $\mathbf{K}_L$, $\mathbf{K}_{\mathrm{CF}}$, $\mathbf{K}_G$ matrices are $n \times n$, and dimensions of $\mathbf{F}_v$, $\mathbf{F}_{\mathrm{CF}}$, $\mathbf{R}(t)$ vectors are $n \times 1$, where n is the degree of freedom.

Further, electric force, $\mathbf{F}_v$ can be written as

$$\mathbf{F}_v = \int_0^l \oint (\mathbf{B}_u)^{\mathrm{T}}\mathbf{P}\mathbf{E}_1 \,\mathrm{d}s\,\mathrm{d}x = \int_0^l \oint (\mathbf{B}_u)^{\mathrm{T}}\mathbf{P}\frac{\mathbf{V}_a}{p_k}\,\mathrm{d}s\,\mathrm{d}x = \mathbf{K}_{\mathrm{av}}\mathbf{V}_a, \tag{26}$$

where $\mathbf{V}_a$ is the voltage vector in actuators.

Then, a negative velocity feedback control algorithm is used to obtain the active damping effect is performed. Generally, piezoelectric sensors and actuators are embedded or attached to composite layer as shown in Fig. 4. Firstly, from the direct piezoelectric effect, the sensor equation can be derived [8,9]. In this study, sensors are thin film-shape materials such as PVDF. Also, since no external electric field is applied to the sensor layer, and as the charge is collected only in the thickness direction in PVDF sensor, only the electric displacement D_3 is of interest. The width of panel being relatively smaller than the length of the panel is a geometric condition allowing the electric displacement of the sensor layer to be derived as

$$D_3 = e_{31}\varepsilon_{xx} = e_{31}\left(U_{,x} - Y\beta_{z,x} + Z\beta_{y,x} + \psi\phi_{,xx}\right). \tag{27}$$

The total charge generated on the sensor surface is the spatial summation of all the point charge on the sensor layer

$$q_s(t) = \sum_{i=1}^{N_s}\sum_{j=1}^{N_p}\int_A D_3\,\mathrm{d}A. \tag{28}$$

Therefore, the current on the surface of a sensor can be presented as

$$i(t) = \frac{\mathrm{d}q_s(t)}{\mathrm{d}t} = \mathbf{K}_{\mathrm{sv}}\dot{\mathbf{q}}. \tag{29}$$

When the piezoelectric sensors are used as strain rate sensors, the current can be converted into the sensor voltage output V_s as

$$V_s = G_c i(t) = G_c\mathbf{K}_{\mathrm{sv}}\dot{\mathbf{q}}, \tag{30}$$

where G_c is the gain of the current amplifier transforming the sensor current voltage.

The distributed sensors generate a voltage when the structures are oscillating and this signal is fed back into the distributed actuator using a control algorithm [8].

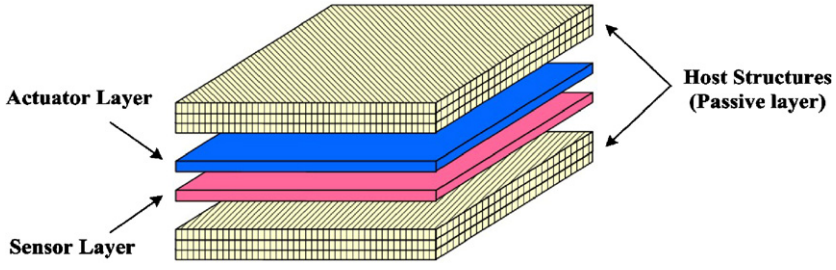

Fig. 4. The position of sensor and actuator layer.

The system actuating voltage can be presented as

$$V_a = G_c G_i \mathbf{K}_{\mathrm{sv}} \dot{\mathbf{q}}, \tag{31}$$

where G_i is the feedback control gain.

In the feedback control, the electric force vector $\mathbf{F}_v$ can be regarded as a feedback force [8]

$$\mathbf{F}_v = \mathbf{K}_{\mathrm{av}} G_c G_i \mathbf{K}_{\mathrm{sv}} \dot{\mathbf{q}}. \tag{32}$$

Let $\mathbf{C}_V = -\mathbf{K}_{\mathrm{av}} G_c G_i \mathbf{K}_{\mathrm{sv}}$. Then, the governing equation considering a negative velocity feedback control becomes:

$$\mathbf{M}\ddot{\mathbf{q}}(t) + (\mathbf{C}_C + \mathbf{C}_V)\dot{\mathbf{q}}(t) + (\mathbf{K}_L + \mathbf{K}_{\mathrm{CF}} + \mathbf{K}_G)\mathbf{q}(t) = \mathbf{F}_{\mathrm{CF}} + \mathbf{R}(t). \tag{33}$$

As shown in this equation, $\mathbf{C}_V$ is the active damping term in the negative feedback control using distributed piezoelectric sensors and actuators. Therefore, the voltage control algorithm applies a damping effect on the vibration control of a distributed system.

2.5. Solution procedure

To obtain the natural frequency, we can derive the perturbed equation [21]. The solution of the equation is separated into static- and time-dependent terms. Then the displacement vector $\mathbf{q}$ may be expressed as $\mathbf{q} = \mathbf{q}_s + \boldsymbol{\delta}(t)$, where $\mathbf{q}_s$ and $\boldsymbol{\delta}(t)$ denote the static solution and a small perturbation about the static equilibrium state, respectively. Thus we can obtain the perturbed equations which take the form as

$$\mathbf{M}\ddot{\boldsymbol{\delta}} + \mathbf{C}\dot{\boldsymbol{\delta}} + \mathbf{K}\boldsymbol{\delta} = \mathbf{0}, \tag{34}$$

where $\mathbf{C} = \mathbf{C}_C + \mathbf{C}_V$ and $\mathbf{K} = \mathbf{K}_L + \mathbf{K}_{\mathrm{CF}} + \mathbf{K}_G$.

To solve this equation, it can be rewritten in the state space form:

$$\mathbf{A}\mathbf{g} - \mathbf{B}\dot{\mathbf{g}} = \mathbf{0}, \tag{35}$$

where

$$\mathbf{A} = \begin{bmatrix} \mathbf{M} & \mathbf{0} \\ \mathbf{0} & \mathbf{K} \end{bmatrix}, \quad \mathbf{B} = \begin{bmatrix} \mathbf{0} & \mathbf{M} \\ -\mathbf{M} & -\mathbf{C} \end{bmatrix} \text{ and } \mathbf{g} = \begin{Bmatrix} \dot{\boldsymbol{\delta}} \\ \boldsymbol{\delta} \end{Bmatrix}.$$

The solution of the above equation is assumed to be of the form $g = \tilde{C}\,\mathrm{e}^{\lambda t}$, where $\tilde{C}$ is an arbitrary constant. As a result, the equation of motion can be simplified as the generalized eigenvalue problem and takes the form as

$$\mathbf{A}\mathbf{g} = \lambda \mathbf{B}\mathbf{g}. \tag{36}$$

The time response of the system is obtained through Newmark time integration method [23].

The equilibrium equations at time $t + \Delta t$ are considered as follows:

$$\mathbf{M}^{t+\Delta t}\ddot{\mathbf{q}} + \mathbf{C}^{t+\Delta t}\dot{\mathbf{q}} + \mathbf{K}^{t+\Delta t}\mathbf{q} = {}^{t+\Delta t}\mathbf{F}. \tag{37}$$

The $\dot{\mathbf{q}}$ and $\mathbf{q}$ at time $t + \Delta t$ are obtained from the $\ddot{\mathbf{q}}$, $\dot{\mathbf{q}}$ and $\mathbf{q}$ at time t, and are written as

$$\begin{aligned} {}^{t+\Delta t}\dot{\mathbf{q}} &= {}^{t}\dot{\mathbf{q}} + \left[(1-\tilde{\delta})\,{}^{t}\ddot{\mathbf{q}} + \tilde{\delta}\,{}^{t+\Delta t}\ddot{\mathbf{q}}\right]\Delta t, \\ {}^{t+\Delta t}\mathbf{q} &= {}^{t}\mathbf{q} + {}^{t}\dot{\mathbf{q}}\Delta t + \left[\left(\frac{1}{2} - \tilde{\alpha}\right){}^{t}\ddot{\mathbf{q}} + \tilde{\alpha}\,{}^{t+\Delta t}\ddot{\mathbf{q}}\right]\Delta t^2, \end{aligned} \tag{38}$$

where $\tilde{\delta}$ and $\tilde{\alpha}$ are the parameters that can be determined to obtain the integration accuracy and stability parameter, and Δt is time interval. $\tilde{\delta} = 0.5$ and $\tilde{\alpha} = 0.25$ are chosen

$$
\begin{aligned}
{}^{t+\Delta t}\mathbf{q} &= \left[\widehat{K}\right]^{-1}\left[{}^{t+\Delta t}\widehat{R}\right],\\
{}^{t+\Delta t}\ddot{\mathbf{q}} &= \frac{1}{\tilde{\alpha}\Delta t^2}\left({}^{t+\Delta t}\mathbf{q} - {}^{t}\mathbf{q}\right) - \frac{1}{\tilde{\alpha}\Delta t}{}^{t}\dot{\mathbf{q}} - \left(\frac{1}{2\tilde{\alpha}} - 1\right){}^{t}\ddot{\mathbf{q}},\\
{}^{t+\Delta t}\dot{\mathbf{q}} &= {}^{t}\dot{\mathbf{q}} + \Delta t\left(1 - \tilde{\delta}\right){}^{t}\ddot{\mathbf{q}} + \tilde{\delta}\Delta t\,{}^{t+\Delta t}\ddot{\mathbf{q}}.
\end{aligned}
\tag{39}
$$

3. Numerical results and discussions

In the numerical study, we considered the effect of feedback control gain, rotating speed, pre-twist angle and fiber orientation in host structures on the response of the rotating composite thin-walled beam. Furthermore, to effectively use active materials, the positions and distribution areas of the sensors and actuators are investigated through a case study. The response of the beam subject a time varying load such as an impulse load or a sinusoidal load are investigated and the change of damping ratio at the first flap and lag mode is presented.

3.1. Code verifications

To verify the code for numerical simulation, the normal mode analysis for the composite thin-walled beam in the rotating condition is performed. In addition, the actuation performance of active beam with piezo-composite actuators is calculated for code verification.

As a first step, the natural frequency of the rotating composite box beam is calculated and it is compared with the previous data. The stacking sequence of the model is $[-30]_6$ in top, $[30]_6$ in bottom, $[30/-30]_3$ in right and left panel, respectively. In this paper, the ply-angle orientation is positive when it is measured from the positive s-axis towards the positive x-axis (see Figs. 1 and 2). Furthermore, the beam is made of graphite-epoxy. Table 1 shows the lowest three natural frequencies for the rotating speed of 1014 rev/min. Also, Fig. 5 presents the change of the natural frequency of anti-symmetric thin-walled beam for the various pre-twist angles. Present results are almost equal to the data in Refs. [3,4,6,7].

In the second step, the actuating performance of piezo-composite materials is examined. The model of the single-cell thin-walled beam with the cross-section of NACA0012 airfoil is used for verification [17]. The AFC which is a piezo-composite materials is embedded between E-glass layers as active materials. Also, the fiber-orientation of AFC pack is 45° to obtain twist control. Fig. 6(a) shows the twist angle at the tip of the active beam under various applied voltages and Fig. 6(b) presents the variation of the twist angle through the span when actuating voltage is 1800 V. The present results were in good agreement with the references.

3.2. Vibration control applied by a negative velocity feedback control

To investigate the active damping effect produced by a velocity feedback control algorithm with distributed piezoelectric sensors and actuators, a rotating composite thin-walled beam as shown in Fig. 1 is considered.

Table 1
Natural frequency at 1014 rev/min

Mode	Experiment		Analysis	Present
	Ref. [3]	Ref. [4]	Ref. [6]	
Flap 1	28.60	28.13	27.33	27.65
Lag 1	39.50	42.85	38.66	42.16
Flap 2	135.0	139.8	133.6	135.7

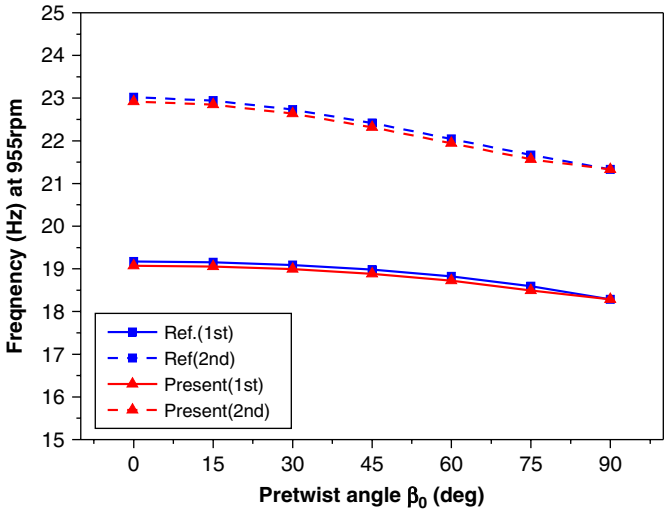

Fig. 5. The variation of frequencies at the various pretwist angles.

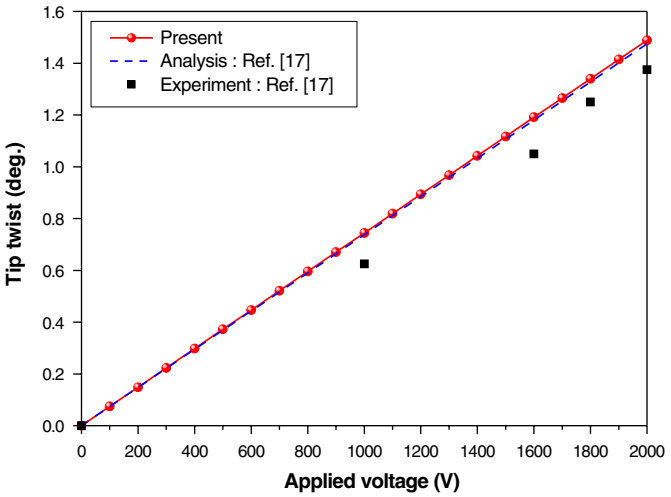

Fig. 6. Tip twist angle for various actuating voltages.

Table 2(a)
Material properties of passive materials

Material properties	Graphite-epoxy
Longitudinal Young's modulus, E_1 (GPa)	141.96
Transverse Young's modulus, E_2 (GPa)	9.79
Shear modulus, G_{12} (GPa)	6.13
Poisson's ratio (v_{12})	0.42
Density, ρ (kg/m^3)	1445
Layer thickness, t (mm)	0.762

Dimensions of length, width, height and hinge offset are 844.5, 23.1, 12.6 mm and 10% of the span, respectively. The host structures are made of graphite-epoxy, while the sensors and actuators are PVDF having a thin film shape and MFC that is piezo-composite materials, respectively. Their material properties are presented in Table 2. Sensors and actuators are embedded between composite layers at the center of the

Table 2(b)
Material properties of active materials

Material properties	PVDF (sensor)	AFC (actuator)	MFC (actuator)
Longitudinal Young's modulus, E_1 (GPa)	2.0	30.535	36.5
Transverse Young's modulus, E_2 (GPa)	2.0	16.105	7.6
Shear modulus, G_{12} (GPa)	0.775	5.5	14.6
Poisson's ratio (v_{12})	0.3	0.454	0.25
Density, ρ (kg/m^3)	1800	4810	7552
Layer thickness, t (mm)	0.1	0.1689	0.23
Electrode space, p (mm)	N/A	1.1	1.0
Piezoelectric strain constant (pm/V)	23.0(d_{31}) 23.0(d_{32})	381(d_{11}) −160(d_{12})	530(d_{11}) −210(d_{12})

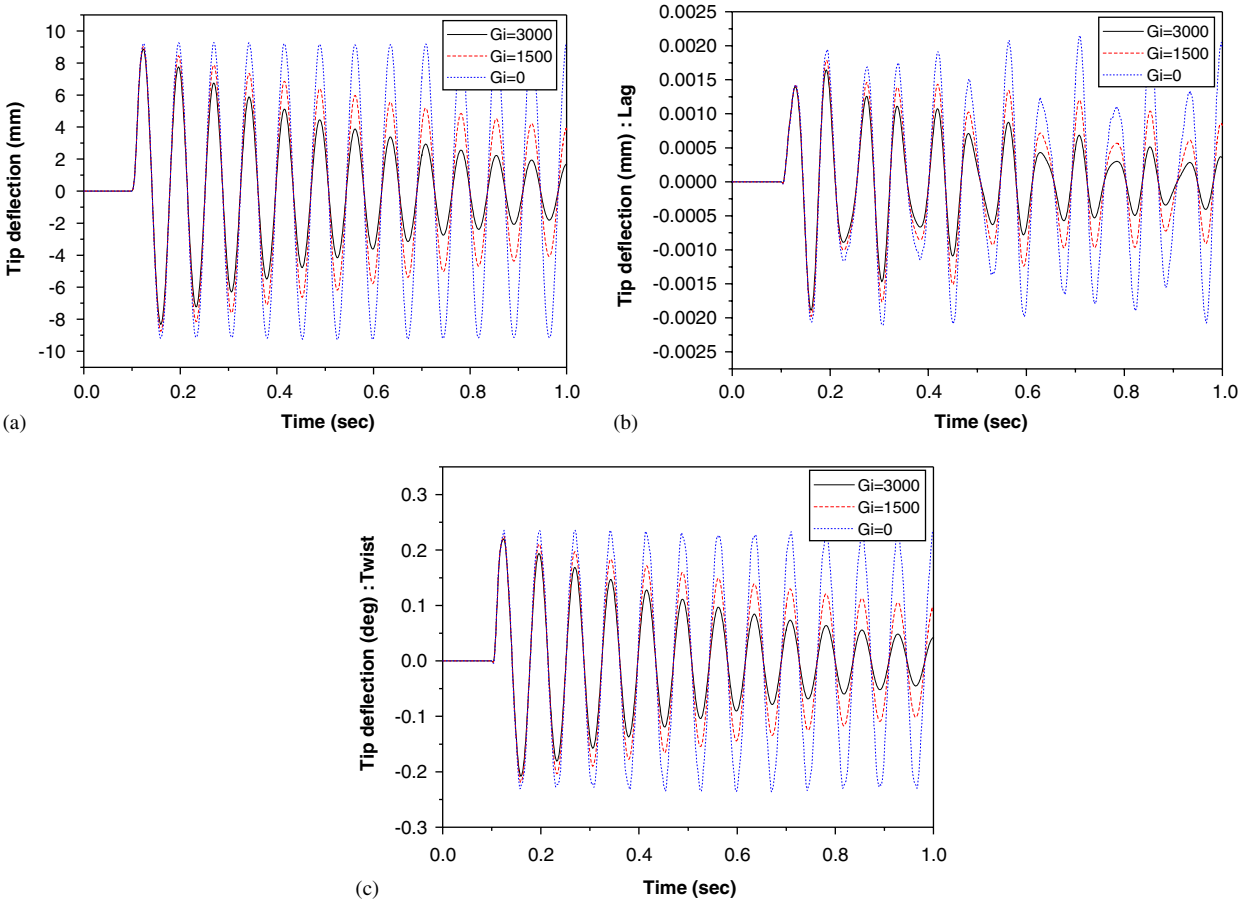

Fig. 7. Time response of symmetric lay-up beam subject to an impulse load.

cross-section. Further, MFC actuators are laminated at 0° with respect to the beam axis for bending control. The stacking sequence of the host structures is $[-30]_6$ in top, $[30]_6$ in bottom, $[30/-30]_3$ in right and left panel, respectively.

Fig. 7 shows the time response of the beam under a Z-directional impulsive load at 0 rev/min. The beam is oscillated to flapping direction by an impulse load. Also, because the beam has elastic coupling effects for flap-lag and bending-torsion in symmetric lay-up, lagging and torsional oscillations are generated. Fig. 7 shows

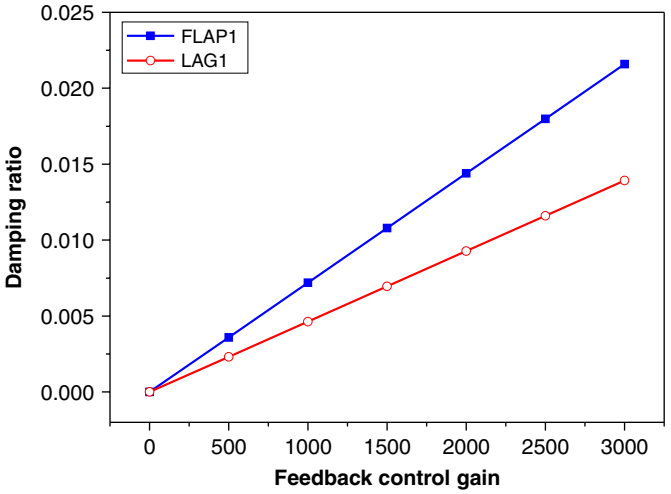

Fig. 8. The variation of damping ratio for various feedback control gains.

that the oscillation in the three directions can be damped out using a negative feedback control algorithm. As the control gain is increased, damping effect is higher and vibrations are decreased quicker.

Fig. 8 shows the variation of the damping ratio at the first flap and lag mode for increasing of feedback control gain. The damping ratio increases constantly as the feedback control gain increases. But, feedback control gain can not be increased infinitely because applied voltage must be limited for the sake of breakdown voltage of actuators.

3.3. *Effects of rotating speed and pre-twisted angle*

Generally, rotating beams like rotor blades, have specific rotating speed for operation. This operating speed varies with the type of system and operating status. Also, most of blades have a pre-twist angle, which is a common design factor of blades. Thus, the damping effect according to the rotating speed and pre-twist angle should be investigated.

Above all, the effect of rotating speed is discussed. The symmetric lay-up beam which is used in Section 3.2 is considered for numerical simulation. Fig. 9 shows the variation of frequencies and damping ratios for the first and second modes when the same feedback control gain ($G_i = 3000$) is applied. Frequencies increase as the rotating speed is increased, because of a larger centrifugal force at a higher rev/min. Conversely, the damping ratio decreases at higher rev/min when the frequency increases. But, the real part of the eigenvalue hardly changes with rotating speed, as shown in Fig. 9(c). Therefore, the absolute damping effect is nearly same between the non-rotating condition and the rotating condition. Fig. 10 shows the time response of the same beam subject to an impulse load when the beam is rotated at 0, 500 and 1000 rev/min. Fig. 10 presents that the initial magnitude of vibration in non-rotating condition is larger than that in the rotating condition. But, the absolute damping effect is almost similar to those of the cases in which the beam is rotated from 0 to 1000 rev/min, because the relative damping ratio of the non-rotating condition is larger than that of the rotating condition.

Secondly, the effect of the pre-twist angle is presented. The pre-twist angle consists of the pre-twist angle per unit length and setting angle of the beam as shown in Fig. 1. Three anti-symmetric lay-up beams are considered to investigate the effect of pre-twist angle per unit length of the beam (β_0). Their stacking sequence of host structures are $[0\ 15\ 0\ 15\ 0\ 15]_T$, $[0\ 30\ 0\ 30\ 0\ 30]_T$ and $[0\ 45\ 0\ 45\ 0\ 45]_T$, respectively. The sensors and actuators are embedded between composite layers at the center of the cross-section. When the same feedback control gain ($G_i = 3000$), setting angle ($\gamma = 0$), and rotating speed (1000 rev/min) are applied, Fig. 11 shows the effect of pre-twist angle of the beam for frequencies and damping ratios at the 1st and 2nd mode. As shown

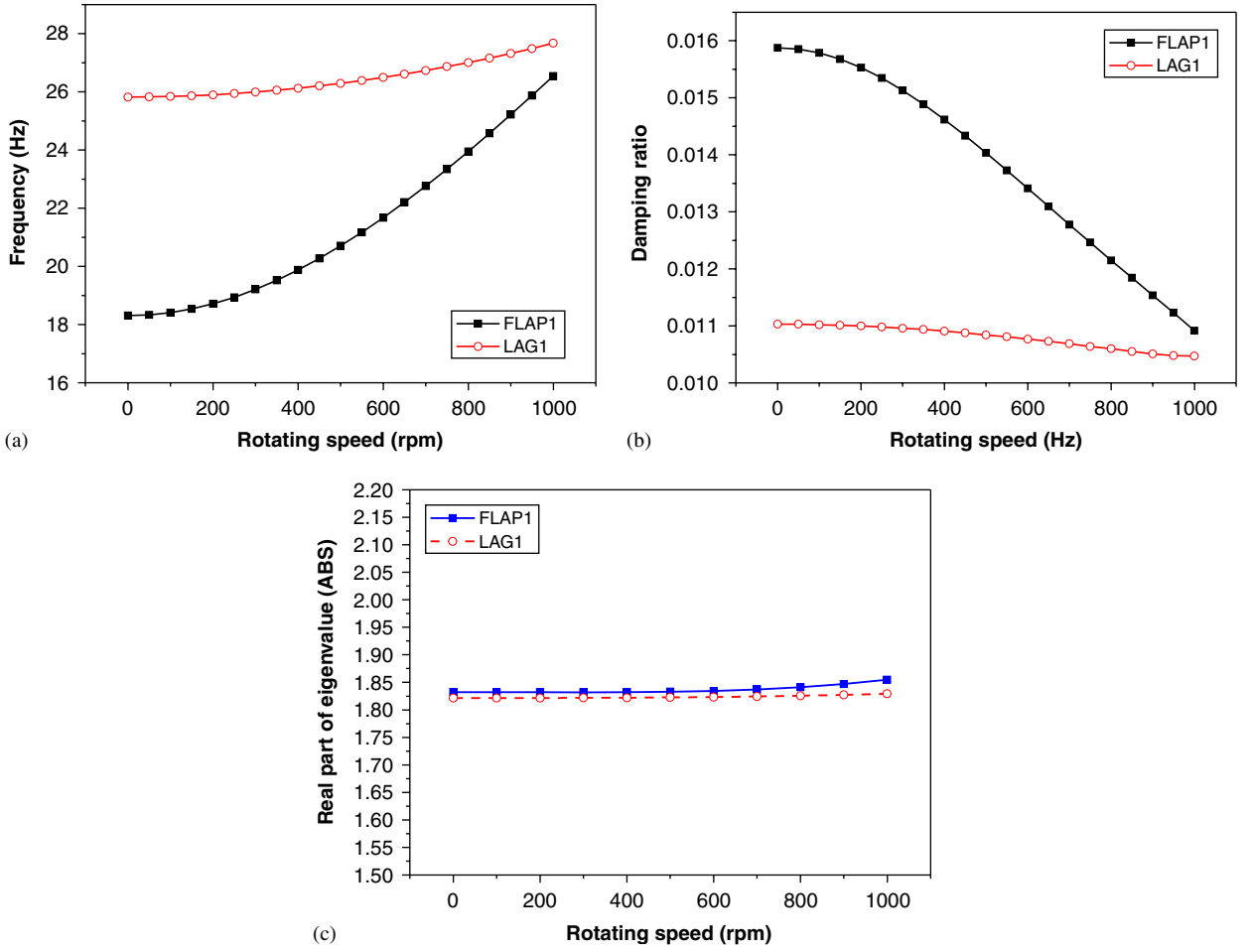

Fig. 9. The variation for the change of rotating speed.

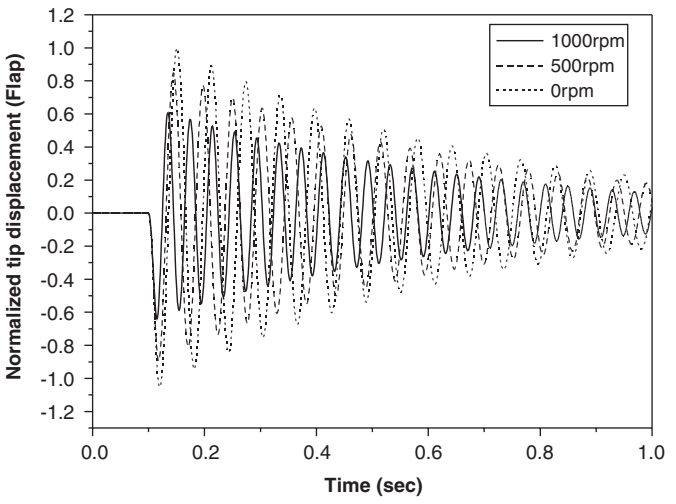

Fig. 10. Time response of beams with 500 and 1000 rev/min subject to an impulse load.

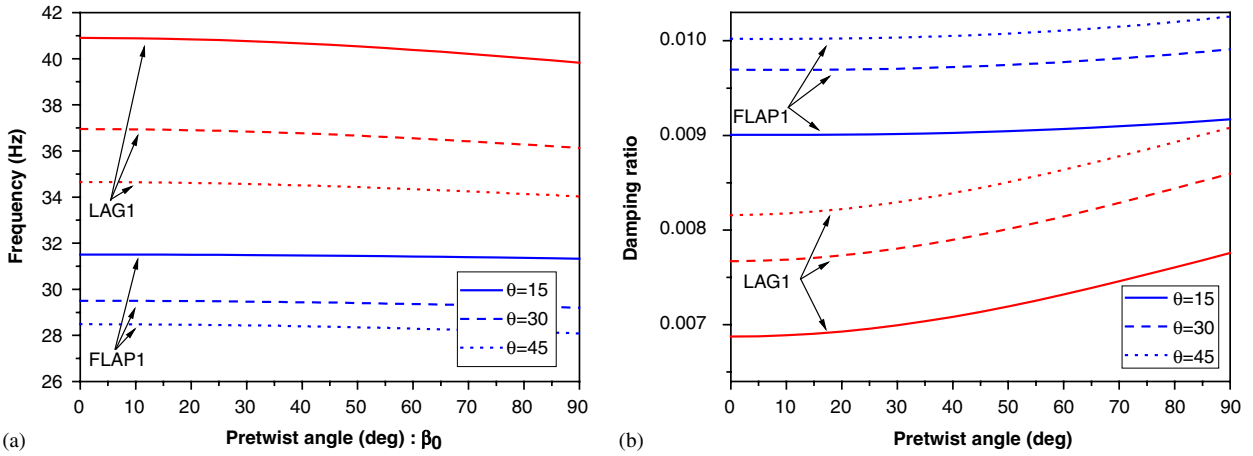

Fig. 11. The effect of pretwist angle per unit length of the blade at 1000 rev/min.

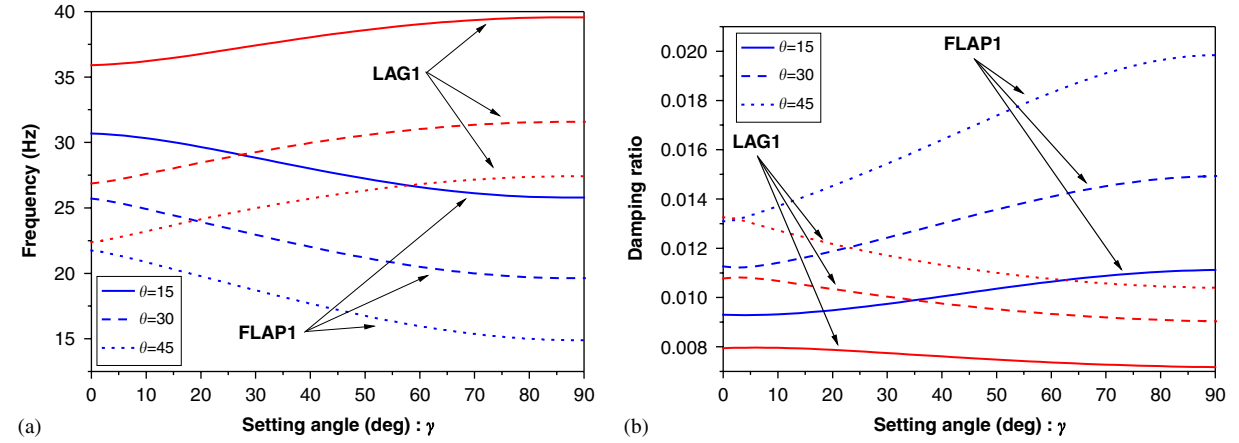

Fig. 12. The effect of setting angle at 1000 rev/min.

in Fig. 11, frequencies decrease and damping ratios increase as the pre-twist angle per unit length of the beam increases.

Also, the effect of setting angle is investigated. The beam which has stacking sequence in host structures $[-\theta]_6$ in top, $[\theta]_6$ in bottom, $[\theta/-\theta]_3$ in right and left panel is considered. Active layers are located at the center of the wall. For the same control gain ($G_i = 3000$), the pre-twist angle per unit length of the beam ($\beta_0 = 0$) and rotating speed (1000 rev/min) are applied, Fig. 12 shows the effect of setting angle of the blade. As the setting angle increases, the frequency of the first flap mode decreases and the frequency of the first lag mode increases. On the other hand, the damping ratio of the first flap mode increases and the damping ratio of the first lag mode decreases. In a general actual blade, the pre-twist angle is not moderately large. So, variation of the damping effect that is induced by the pre-twist angle is smaller than those of other factors.

3.4. The effect of ply-angle in host structures

Fiber orientation of composite materials is a very important design factor for composite thin-walled beams. Generally, the variation of the ply-angle in host structures affects the frequency, and the change of the frequency influences to the damping effect that is obtained through a negative velocity control.

First of all, three cases of a beam each possessing different lay-up types are considered. Case 1 ($[0\ \theta\ 0\ \theta\ 0\ \theta]$) and Case 2 ($[\theta]_6$) are an anti-symmetric lay-up beam and Case 3 ($[-\theta]_{6\,\mathrm{top}}$, $[\theta]_{6\,\mathrm{bottom}}$, $[\theta/-\theta]_{3\,\mathrm{right\&left}}$) is

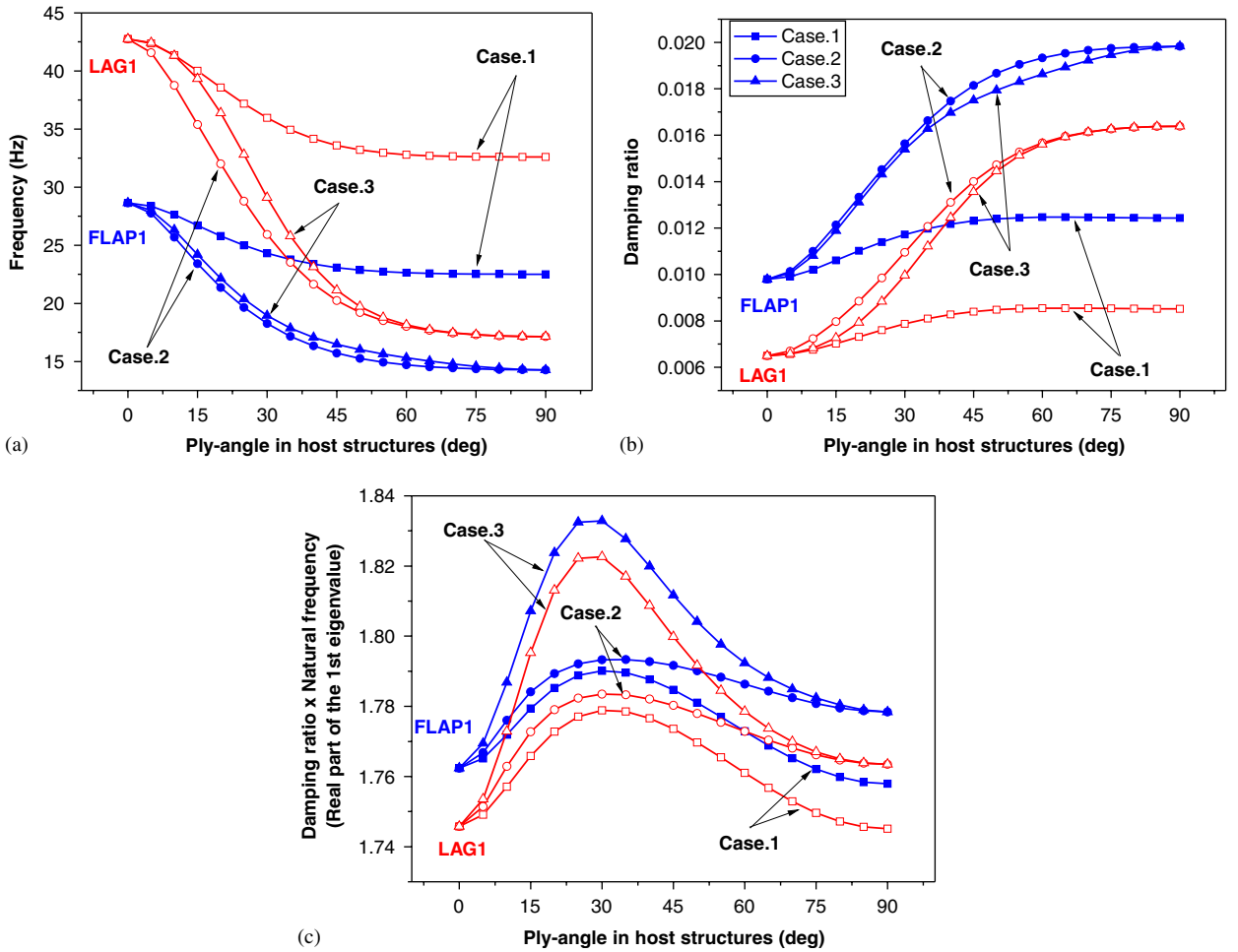

Fig. 13. The effect of ply-angle in host structures at various rotating speeds.

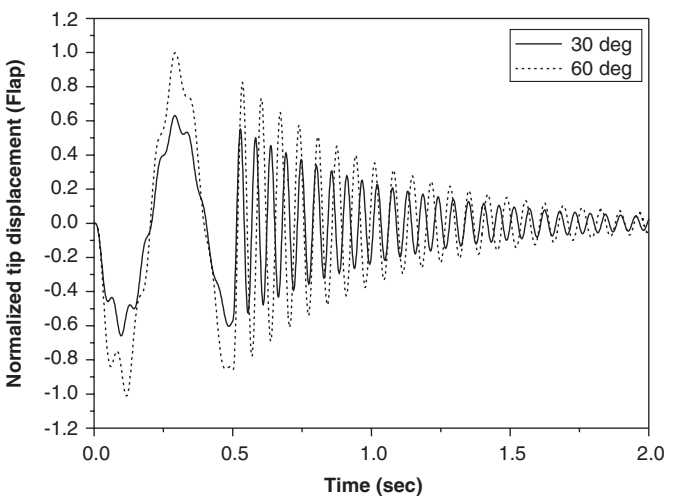

Fig. 14. The variation of time response subject a sinusoidal load for the change of ply-angle.

a symmetric lay-up beam. When the same control gain ($G_i = 3000$) and rotating speed (500 rev/min) are applied, the influence of the change of ply-angle in the host structures is shown in Fig. 13. As the ply-angle in host structures decreases, the frequencies of the beam increases, and damping ratios decrease as shown in Fig. 13(a) and (b). This result is induced because the bending stiffness of beams becomes larger at a smaller ply-angle in the host structures. Also, the absolute damping effect is the highest when beams have the fiber-orientation of 30°. These results confirmed that the symmetric lay-up beam has a higher damping performance than the anti-symmetric lay-up beam. Fig. 14 presents the variation in response for the change of the ply-angles in the host structure under a sinusoidal load $\left(f = f_0 \sin(5\pi t)\right)$ for certain time. In this example, the duration of the sinusoidal load is 0.5 s. Lay-up type of beams in passive structures is anti-symmetric $[\theta]_6$. The same feedback control gain ($G_i = 3000$) and rotating speed (1000 rev/min) are applied. Fig. 14 shows that the initial magnitude of vibration is decreased as the ply-angles of composite are decreased. These results indicate that the frequency and damping ratio have a inverse relation. If the frequency is increased, the damping effect is decreased. Further, the active damping performance can be increased through the proper structural tailoring of the composite materials that are passive structures.

3.5. *The influence of the position and area of sensor/actuator pair*

The position and area of the sensor/actuator pair are important factors for effective vibration reduction in an active beam. Because of the high cost of piezoelectric sensors and actuator, suitable arrangements for

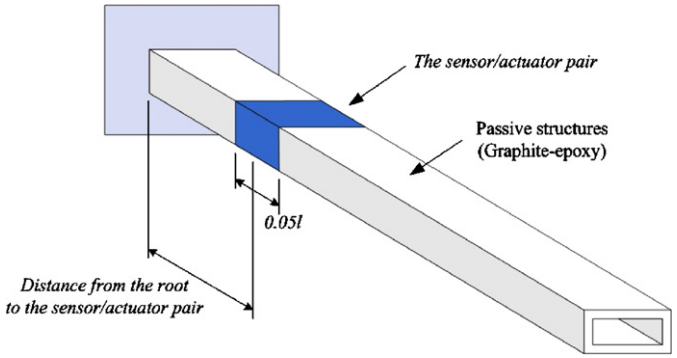

Fig. 15. The position of sensor and actuator pair.

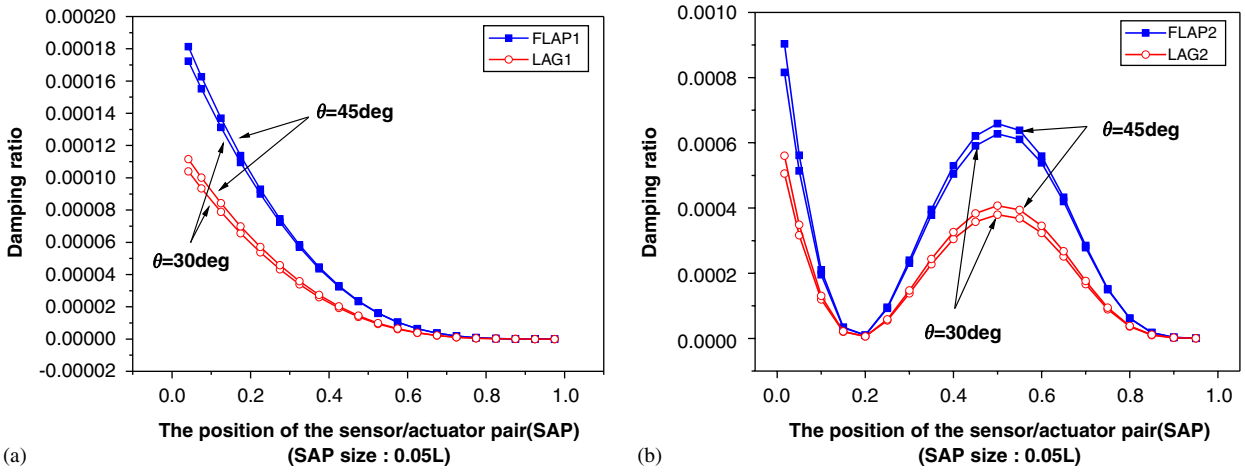

Fig. 16. The variation of damping ratio for the position of sensor and actuator pair.

position and the distributed area of sensor/actuator pair need to be discussed for economical use of active materials.

Initially, the beam as shown in Fig. 15 is considered to investigate the influence of the position of sensor/actuator pair. The beam at 1000 rev/min has a symmetric lay-up and the stacking sequences in host structure are $[-\theta]_6$ in top, $[\theta]_6$ in bottom, $[\theta/-\theta]_3$ in right and left panel, respectively. Also, the size of sensor/actuator pair is 5% of the total surface area of the considered thin-walled beam. When the position of the sensor/actuator pair is changed from the root to tip of beam, damping ratios of the first flap and lag mode are calculated in Fig. 16(a). Damping effect is the highest when sensor/actuator pair is located near the root of the beam. But, as the position of sensor/actuator pair is moved to the tip, the damping performance is decreased dramatically. When the sensor/actuator pair is located over about 80% of the beam span from the root, the damping effect is nearly zero. Because the first flap and lag modes are the most important mode to bending control of the beam, the sensor/actuator should be located near the root to obtain better vibration control performance. Also, the sensor/actuator pair near the tip of beam is invalid as an active structure. Further, Fig. 16(b) shows damping ratios of the second flap and lag mode. Damping ratio of the sensor/actuator pair located near the root and about 50% span is larger than that of the sensor/actuator pair at another position. But, the contribution of the first modes is much larger than another higher mode in the case of the slender beam. Therefore, the sensor/actuator pair at the root of beam yields more effective damping than that at another location.

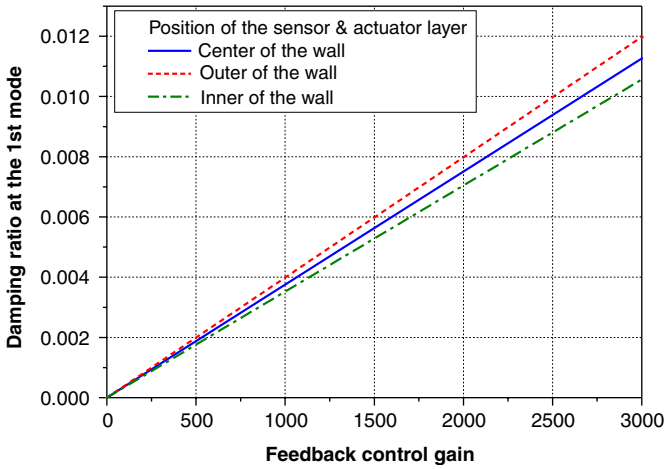

Fig. 17. The variation of damping ratio for the position of active layer.

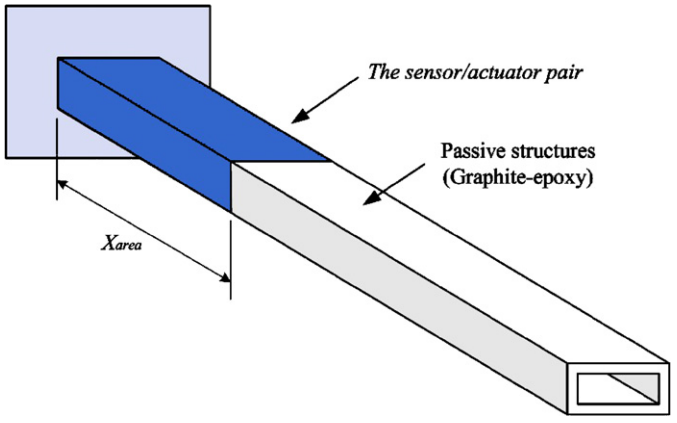

Fig. 18. The distributed area of sensor and actuator pair.

Secondly, the influence of the position of the active layer that contains the sensor/actuator pair is considered. Beams are rotated at 1000 rev/min. Three cases where the active layers are located at the outer, center and inner section of the beam wall, respectively, are investigated in Fig. 17. Also, the active layer located at the outer side shows the highest damping effect in the three cases for the same feedback control gain. This is because the active layer at the outside has a larger bending force for actuation than in the case in which the active layer is located inside.

Thirdly, the symmetric lay-up beam in Fig. 18 is considered to discuss the influence of the distribution area of the sensor/actuator pair. And, the effect of the change of the active area is calculated in the non-rotating condition. As shown in Fig. 19, when the area of the sensor/actuator pair increases from 5% to 100% of the total surface area, damping ratios usually increase. But, as the active area is increased to over about 80% of the total surface area, the damping ratio is decreased slightly as shown in Fig. 19(b). This is because the sensor/actuator pairs near the tip is invalid as an active structure and they only act like added mass at the tip. Therefore, actuators near the tip of the beam (about 80–100% of span) have a negative effect on the damping performance. In addition, as the area of sensor/actuator pair is changed, frequencies are changed, as shown in Fig. 19(a). As the decreasing of the frequency in structures need to be eluded generally, suitable active area for considering the first flap and lag mode is approximately 70% of the total surface area as shown Fig. 19(c). Further, Fig. 20 shows the influence of sensor/actuator position in the alternative case. The passive material has the stacking sequence in Section 3.2 with the rotating speed at zero. The first fixed sensor/actuator pair that is located basically in the 0–30% span. And, the position of the second sensor/actuator pair that has a size 10% of total surface area is changed from 35% to 95% span. As shown in Fig. 18, when the second

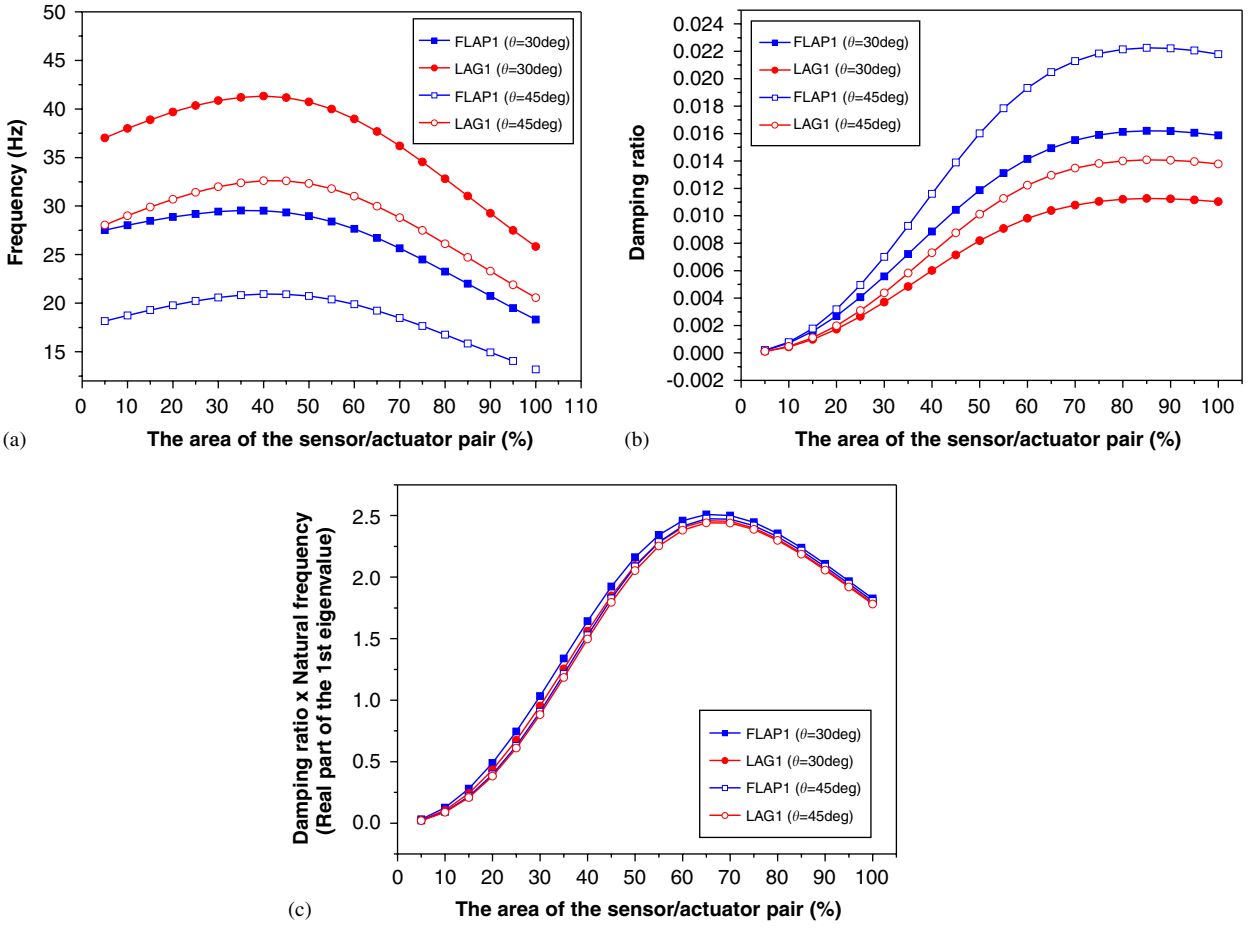

Fig. 19. Influence of the active area (Case A).

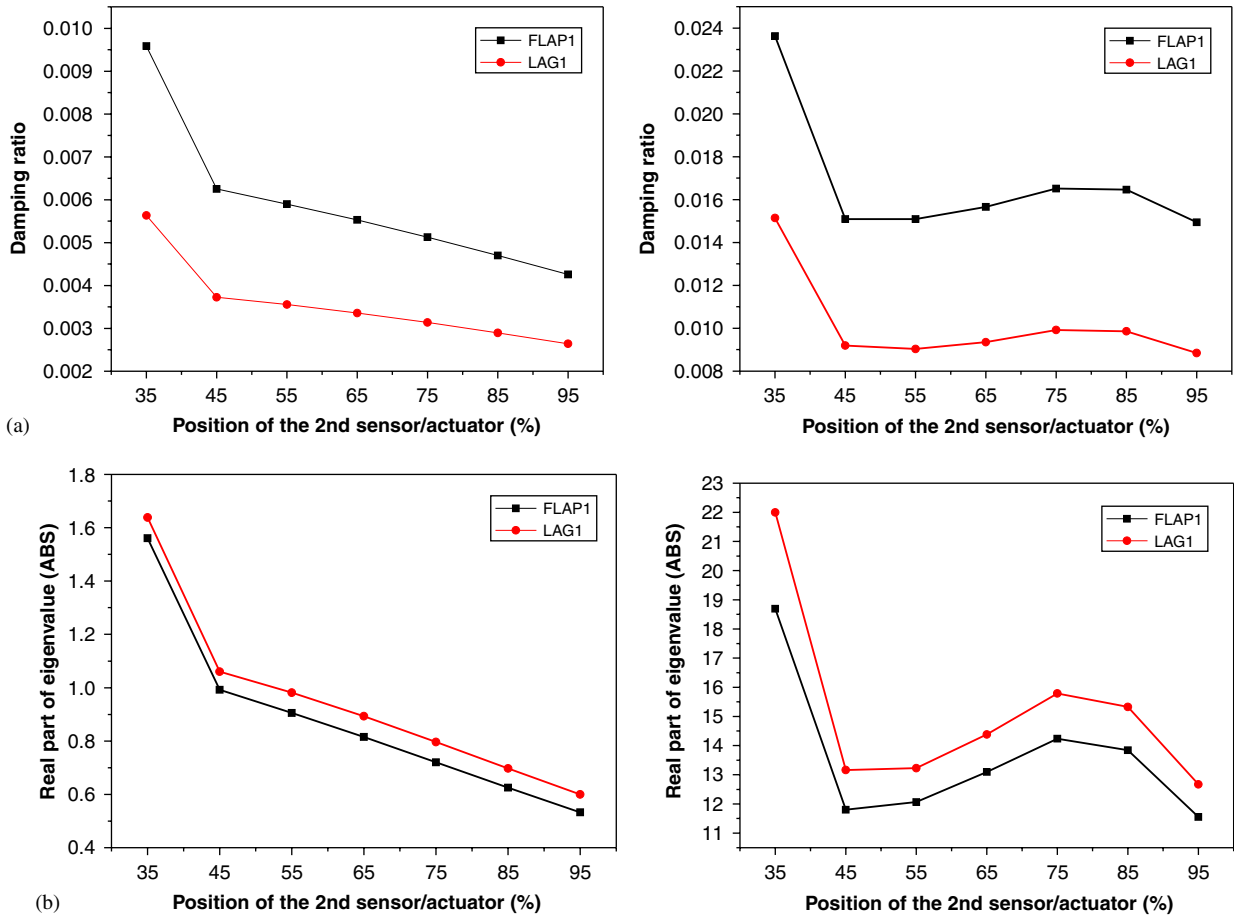

Fig. 20. The influence of active area (Case B).

sensor/actuator pair is near the root of the beam, damping effect is larger. It is induced that the beam has a slender shape. Thus, active materials near the root have more advantage than other cases.

Generally, the cost of active materials rises as the mass of the system increases with use of more actuators. So, adequate vibration suppression performance will be obtained through the proper arrangement and distribution size of the sensor/actuator pair.

4. Conclusions

Vibration control of the pre-twisted rotating composite thin-walled beam with MFC actuators and PVDF sensors is studied. The results in this study illustrate that an active damping effect can be obtained through negative velocity feedback control algorithm with PVDF sensors and MFC actuators. The active damping effect has linearly related to the feedback control gain, so vibrations can be damped out quicker when the higher feedback control gain is applied within the limit of the actuator voltage. Rotating beams like blades are operated at a specific rotating speed, and they have pre-twist angle, generally. As the rotating speed is increased, the frequency is increased. Accordingly, the damping ratio is decreased as the rotating speed is increased. But, the absolute damping effect is nearly same between the non-rotating condition and rotating condition. Also, the damping effect is changed, as pre-twist angle is increased. The influence for the pre-twist angle is relatively smaller than that of rotating speed.

In addition, the fiber-orientation of composite materials in the host structures affects the damping performance of the active beam. As the ply-angle is increased, the damping ratio is increased, generally. This is due to the fact

that the bending stiffness decreases as ply-angle increases. Therefore, the damping effect can be increased through the adequate structural tailoring of passive structures made of composite materials. Accordingly, adequate vibration suppression performance will be obtained through the suitable arrangement and distribution size of sensor/actuator pair. Also, it is confirmed that the optimal design and the optimal control theory need to be studied for obtaining the optimal damping effect of rotating composite thin-walled beam. This research with PVDF sensors and MFC actuators can be applied to enhance the damping performance for vibration suppression of helicopter blades, tilt-rotor aircraft blades, flexible robot arms and wind turbine, etc.

The focus of this research is to obtain active damping effects using piezoelectric fiber composite materials rather than general piezoelectric materials in structural viewpoint. In future work, more realistic controller design is needed for practical implementation.

References

[1] L.W. Rehfield, Design analysis methodology for composite rotor blades, *Proceedings of the Seventh DOD/NASA Conference on Fibrous Composites in Structural Design*, AFWAL-TR-85-3094, June 1985, pp. 1–15.
[2] L.W. Rehfield, A.R. Atilgan, D.H. Hodges, Nonclassical behavior of Thin walled composite beams with closed cross sections, *Proceedings of the American Helicopter Society National Technical Specialists Meeting: Advanced Rotorcraft Structures*, Williamsburg, VA, October 1988, pp. 42–50.
[3] R. Chandra, I. Chopra, Experimental-theoretical investigation of the vibration characteristics of rotating composite box beams, *Journal of Aircraft* 29 (4) (1992) 657–664.
[4] E.C. Smith, I. Chopra, Aeroelastic response, loads and stability of a composite rotor in forward flight, *AIAA Journal* 31 (7) (1993) 1265–1273.
[5] O. Song, L. Librescu, Free vibration of anisotropic composite thin-walled beams of closed cross-section contour, *Journal of Sound and Vibration* 167 (1) (1993) 129–147.
[6] A.D. Stemple, S.W. Lee, A finite element model for composite beams undergoing large deflection with arbitrary cross-section warping, *International Journal of Numerical Method in Engineering* 28 (9) (1989) 2143–2160.
[7] S.Y. Oh, O. Song, L. Librescu, Effects of pretwist and presenting on coupled bending vibration of rotating thin-walled composite beams, *International Journal of Solid and Structures* 40 (2003) 1203–1224.
[8] J.N. Reddy, On laminated composite plate with integrated sensors and actuators, *Engineering Structures* 21 (1999) 568–593.
[9] K.Y. Lam, X.Q. Peng, G.R. Liu, J.N. Reddy, A finite-element modeling for piezoelectric composite laminates, *Smart Materials and Structures* 6 (5) (1997) 583–591.
[10] A. Mukherjee, S.P. Joshi, A. Ganguli, Active vibration control of piezolaminated stiffened plates, *Composite Structures* 55 (4) (2002) 435–443.
[11] O. Song, L. Librescu, S.Y. Oh, Vibration of pretwisted adaptive rotating blades modeled as anisotropic thin-walled beams, *AIAA Journal* 39 (2) (2001) 285–295.
[12] N.K. Chandiramani, L. Librescu, V. Saxena, A. Kumar, Optimal vibration control of a rotating composite beam with distributed piezoelectric sensing and actuation, *Smart Materials and Structures* 13 (2004) 433–442.
[13] J. Koldoff, A. Chattopadhyay, C. Nam, Active control of composite box beams using in-plane piezoelectric actuation and structural coupling with optimization, *Proceedings, SPIE, Smart Structures and Integrated Systems*, Vol. 3985, March 2000, pp. 130–139.
[14] S.-B. Choi, M.S. Han, Vibration control of a rotating cantilevered beam using piezoactuator: experimental work, *Journal of Sound and Vibration* 277 (2004) 436–442.
[15] A. Bent, Active fiber composite material systems for structural control applications, *Proceedings, SPIE's Sixth International Symposium on Smart Structures and Materials*, Newport Beach, CA, March 1–5.
[16] W. Wilkie, J. High, P. Mirick, R. Fox, B. Little, R. Bryant, R. Hellbaum, A. Jalink, Low-cost piezocomposite actuator for structural control applications, *Proceedings, SPIE's Seventh International Symposium on Smart Structures and Materials*, Newport Beach, CA, March 5–9, 2000.
[17] A.d. Plessis, N.W. Hagood, Modeling and Experimental Testing of Twist Actuated Single Cell Composite Beam for Helicopter Blade Control, Master Degree Thesis, Massachusetts Institute of Technology, Cambridge, MA, 1996.
[18] Carlos E.S. Cesnik, S.J. Shin, On the twist performance of a multiple-cell active helicopter blade, *Smart Materials and Structures* 10 (2001) 53–61.
[19] E.F. Sheta, R.W. Moses, L.J. Huttsell, V.J. Harrand, Active control of F/A-18 vertical tail buffeting using piezoelectric actuators, *Proceedings of the 44th AIAA/ASME/ASCE /AHS/ASC Structures, Structural Dynamics & Materials Conference*, AIAA 2003-1887, Norfolk, VA, April 7–10, 2003.
[20] R.M. Jones, *Mechanics of Composite Materials*, Taylor & Francis, London, 1999.
[21] Y.J. Kee, J.H. Kim, Vibration characteristics of initially twisted rotating shell type composite blades, *Composite Structures* 64 (2) (2004) 151–159.
[22] O. Song, L. Librescu, Structural modeling and free vibration analysis of rotating composite thin-walled beams, *Journal of the American Helicopter Society* 42 (4) (1997) 358–369.
[23] K.J. Bathe, *Finite Element Procedure*, Prentice-Hall, Englewood Cliffs, NJ, 1996.